MRS Advances © 2017 Materials Research Society
DOI: 10.1557/adv.2017.430

Developing a Crystal Plasticity Model for Metallic Materials Based on the Discrete Element Method

Agnieszka Truszkowska[1,2], Qin Yu[1], Peter Alex Greaney[3], T. Matthew Evans[2], Jamie J. Kruzic[4]

[1]School of Mechanical, Industrial, and Manufacturing Engineering, Oregon State University, Corvallis, USA
[2]School of Civil and Construction Engineering, Oregon State University, Corvallis, USA
[3]Department of Mechanical Engineering, University of California Riverside, Riverside, USA
[4]School of Mechanical and Manufacturing Engineering, UNSW Sydney, Sydney, Australia

ABSTRACT

Failure of metallic materials due to plastic and/or creep deformation occur by the emergence of necking, microvoids, and cracks at heterogeneities in the material microstructure. While many traditional deformation modeling approaches have difficulty capturing these emergent phenomena, the discrete element method (DEM) has proven effective for the simulation of materials whose properties and response vary over multiple spatial scales, e.g., bulk granular materials. The DEM framework inherently provides a mesoscale simulation approach that can be used to model macroscopic response of a microscopically diverse system. DEM naturally captures the heterogeneity and geometric frustration inherent to deformation processes. While DEM has recently been adapted successfully for modeling the fracture of brittle solids, to date it has not been used for simulating metal deformation. In this paper, we present our progress in reformulating DEM to model the key elastic and plastic deformation characteristics of FCC polycrystals to create an entirely new crystal plasticity modeling methodology well-suited for the incorporation of heterogeneities and simulation of emergent phenomena.

INTRODUCTION

Improving the accuracy and predictive power of solid deformation models will require inclusion of the underlying micromechanical phenomena of deformation and failure. Such micromechanistic models could help address outstanding issues in the mechanics of materials, such as estimating a material's lifespan [1]. The discrete element method (DEM), originally developed for granular mechanics [2], has potential to provide a robust framework for such models. DEM is inherently heterogeneous in structure and local properties and the simulated elements are distinct entities. Like other discrete methods [3], DEM can readily model the emergence of discontinuities, such as cracks, in a material, which can be challenging for continuum methods, requiring increased complexity and computational cost [4]. Finally, the DEM formulation is similar to molecular dynamics, thus creating possibilities for straightforward implementation of atomistic findings in a macroscale deformation model. In this regard, DEM can serve as a mesoscale modeling method between atomistic and macroscopic whereby each element represents a domain of material consisting of many atoms while maintaining varying levels of local and micromechanical heterogeneity.

To date, DEM has been successful in modeling various plasticity and damage-related phenomena in granular materials such as soil and rock, including deformation [5], fracture [6], and creep [7]. The method was also adapted to model brittle, amorphous continuum materials such as ceramics [8] and composites [9]. This work presents progress on modifying DEM to model continuum, elastic-plastic deforming materials. In this paper, recent advances are summarized including modeling anisotropic cubic crystal elasticity and isotropic plasticity, the latter both with and without strain hardening. The long-term goal of this effort is to develop a new type of crystal plasticity model for metals and alloys that correctly captures the emergence of deformation and failure mechanisms such as shear bands, voids, cracks, etc.

THEORY

Deformation in the discrete element method

The discrete element method was first developed by Cundall [2]. The model consists of three dimensional spherical elements bonded by spring-like bonds (Figure 1a-b). Elements are randomly packed into an assembly of a desired shape and they can be fused into continuous solid by forming a network of bonds between neighboring elements.

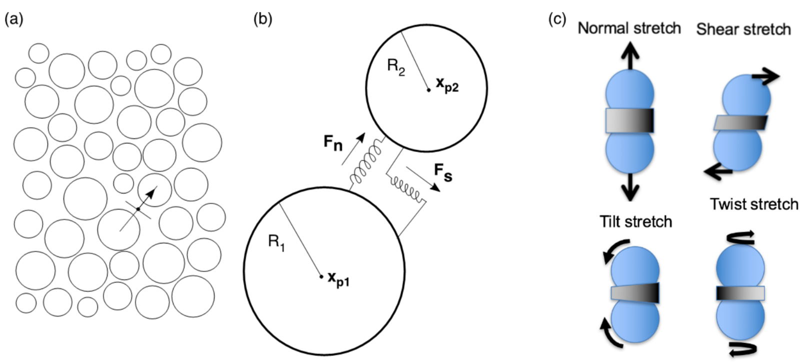

Figure 1. DEM components: (a) DEM assembly of spherical elements, (b) interelement bond represented as a normal and shear spring with each corresponding to the two bond force components, $\mathbf{F_n}$ and $\mathbf{F_s}$ respectively, (c) four basic motions of two bonded elements relative to each other.

At each time step, a DEM simulation proceeds by computing new positions and rotational displacements of elements from their effective forces and moments. These in turn originate from pairwise interactions between bonded elements that impart normal and tangential (shear) forces acting on the element center, along with moments transmitted by tilting and twisting of bonds (Figure 1c). In the present work, deformation was carried solely by the bonds as element stiffnesses were set to zero to ensure the same response of the assembly in tension and compression. A fictitious viscous damping force is also applied to elements to damp out internal vibrations and keep element motion quasistatic.

Elastic deformation of the assembly may occur by stretching, twisting, tilting, and shearing of interelement bonds. Bonds can elastically change shape due to normal or shear forces, resulting in any combination of the four basic deformation modes shown in Figure 1c. In addition to the four modes of elastic deformation, bonds can be allowed to break when either its shear or normal stress exceeds a maximum critical value. In our simulations, a broken bond is permitted to reform up to a user-defined maximum displacement to give permanent bond failure. After the maximum allowed element separation is achieved, the bond remains broken creating damage as a crack or void. We treat this value as a calibration parameter, although it does have physical meaning and is related to the extent of allowable plasticity. Simulations were performed using the software *PFC^{3D}* v5.0 (Itasca Consulting Group, Inc., Minneapolis, MN, USA).

Anisotropic elasticity of cubic materials

Anisotropic cubic elasticity was introduced into DEM by defining angularly dependent bond normal and shear stiffness parameters. The relations for angular dependency were constructed based on spheroid distributions while maintaining cubic symmetry and ensuring rotational invariance of the resultant stiffness tensor. The distribution was a simplification of the normal and shear stiffness distributions typical of cubic materials (Figure 2). Cubic materials with Zener ratio (*Z*) lower than 1 have higher normal stiffness along the <100> direction than the <111> direction, while the opposite holds for materials with $Z > 1$. To mimic this behavior, two spheroid distributions were developed, one with three spheroids aligned along <100> and one with four aligned along <111> (Figure 3). The model simplified the shear stiffness in cubic materials by using only one effective shear direction.

A single cubic material model used two different spheroid stiffness distributions, one for normal and one for shear. This resulted in three unknown parameters that could be fitted to reproduce elastic response of a given cubic material. Elastic response was evaluated based on the stiffness tensor resulting from shear and compressive deformation of a DEM assembly.

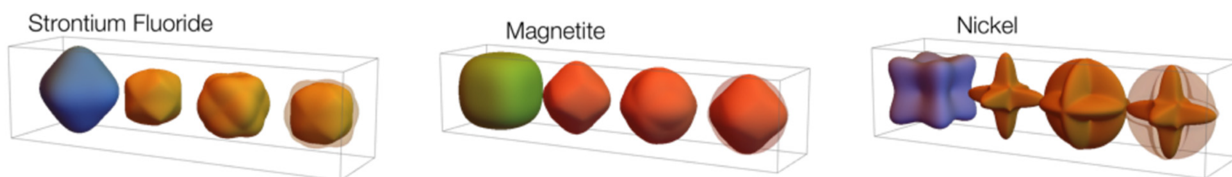

Figure 2. Normal and shear stiffnesses of cubic materials. In each plot the left most subplot is the directionally dependent normal stiffness, the middle two subplots are the shear stiffnesses along the soft and stiff shear directions, and the right most subplot the overlaid shear stiffnesses.

a)

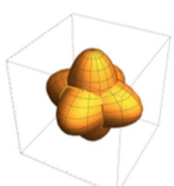

$$r_{i1} = a_i^{\frac{2}{3}} \left(\sqrt{n_x^2 + (n_y^2 + n_z^2) a_i^2} \right)^{-1}$$

$$r_{i2} = a_i^{\frac{2}{3}} \left(\sqrt{n_y^2 + (n_x^2 + n_z^2) a_i^2} \right)^{-1}$$

$$r_{i3} = a_i^{\frac{2}{3}} \left(\sqrt{n_z^2 + (n_y^2 + n_x^2) a_i^2} \right)^{-1}$$

$$r_i = \max(r_{i1}, r_{i2}, r_{i3})$$

$$k_i = A_b / L_b r_i \bar{k}_l$$

b)

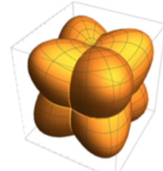

$$r_{j1} = a_j^{\frac{2}{3}} \left(\sqrt{\frac{1}{3} \left((n_x - n_y + n_z)^2 + 2.0(n_x^2 + n_x n_y + n_y^2 - n_x n_z + n_y n_z + n_z^2) a_j^2 \right)} \right)^{-1}$$

$$r_{j2} = a_j^{\frac{2}{3}} \left(\sqrt{\frac{1}{3} \left((n_x + n_y - n_z)^2 + 2.0(n_x^2 - n_x n_y + n_y^2 - n_x n_z + n_y n_z + n_z^2) a_j^2 \right)} \right)^{-1}$$

$$r_{j3} = a_j^{\frac{2}{3}} \left(\sqrt{\frac{1}{3} \left((-n_x + n_y + n_z)^2 + 2.0(n_x^2 + n_x n_y + n_y^2 - n_x n_z - n_y n_z + n_z^2) a_j^2 \right)} \right)^{-1}$$

$$r_{j4} = a_j^{\frac{2}{3}} \left(\sqrt{\frac{1}{3} \left((n_x + n_y + n_z)^2 + 2.0(n_x^2 - n_x n_y + n_y^2 - n_x n_z - n_y n_z + n_z^2) a_j^2 \right)} \right)^{-1}$$

$$r_j = \max(r_{j1}, r_{j2}, r_{j3}, r_{j4}), \qquad k_j = A_b / L_b r_j \bar{k}_l$$

Figure 3. Three (a) and four (b) spheroid distributions – mathematical formulation and example of angular dependence. a_i and a_j are material-dependent parameters that govern the spheroid shape, while k_l is the third parameter that determines the magnitude of resulting stiffnesses.

Isotropic non-hardening plasticity

Isotropic non-hardening plastic deformation under tension is a property of some amorphous materials, such as metallic glasses [10, 11]. To model this behavior with DEM, bonds were reformed with no accompanying change in their tensile and shear strength. The assembly shape resembles an actual tensile testing specimen to avoid stress concentrations near the grips (Figure 4a). The deformation was quasi-static and driven by application of fixed axial velocities to elements on the top and bottom of the specimen.

 https://doi.org/10.1557/adv.2017.430

In addition to reporting stress-strain response, two techniques were developed to assess deformation localization in the assembly: d_2^{min} (the L2 norm of the difference between expected continuum deformation of each point and the simulated DEM deformation) and local cage deformation (the deformation of an imaginary "cage" built around each element, with nodes representing element neighbors (Figure 4a)). The former measures non-affine deformation while the latter provides a method to visualize strain localization into shear bands.

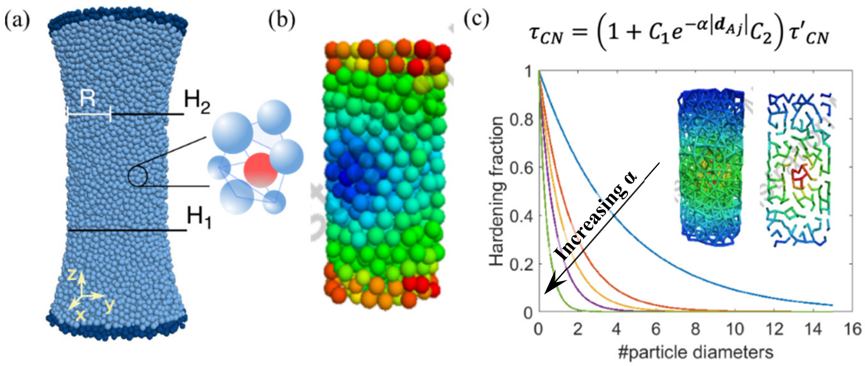

Figure 4. (a) Assembly for tensile testing simulation; (b) Small assembly for probing the exponential decay hardening scheme; (c) Exponential decay hardening scheme – plot shows the range of hardening under different decay parameters and an example hardening distribution in the assembly.

Isotropic plasticity with hardening

A DEM model of plasticity with hardening was created by increasing the strength of a bond each time it is broken and reformed. For the hardening simulations, the bonds were allowed only to break in shear to simulate plastic slip. Three different schemes of hardening were used: (i) hardening only the reformed bond by 1.6% or 3%; (ii) hardening the reformed bond plus nearest neighboring bonds by 0.2%; (iii) hardening bonds in the vicinity of the reformed bond according to an exponential hardening distribution that decays from 1.6% with attenuation length alpha ranging from α = 2 – 20, as shown in Figure 4 (c) . To verify the influence of these hardening schemes on the model, two assemblies were used – one regular sized assembly shown in Figure 4a and a smaller cylindrical assembly shown in Figure 4b. Both assemblies produced similar average stress-strain responses, but the latter had much shorter simulation times.

RESULTS AND DISCUSSION

Anisotropic elasticity of cubic materials

The anisotropic elastic DEM model was used to determine how the spheroid bond stiffness parameters affected the cubic stiffness tensor (Figure 5). The assembly (Figure 5b) was elastically deformed in the ε_{yy} and ε_{xz} strain directions. Figure 5a shows the domain of elastic constants that the model can access in comparison to some real cubic materials [12]. The model captures the behavior of numerous cubic materials but it is also clearly limited. Accessibility of the entire space of anisotropic elastic constants for cubic metals and ceramics is a topic of ongoing work.

Isotropic non-hardening plasticity

The stress-strain responses of the non-hardening simulations are shown in Figure 6a. Three different cases were tested: (1) bonds are much stronger in shear than in tension; (2) bonds strengths are similar in shear and in tension; and (3) bonds are much weaker in shear than in tension. The stress-strain responses had limited plastic elongation, typical of non-hardening ductile materials in tension (e.g., metallic glasses [10]). Case 3, which promoted shear plasticity, reached the highest plastic strains before fracture. Figure 6b shows results of the d_2^{min} analysis which emphasizes the non-affine deformation in the assembly that is characteristic of amorphous materials like metallic glasses. The local cage deformation results shown in Figure 6c indicate

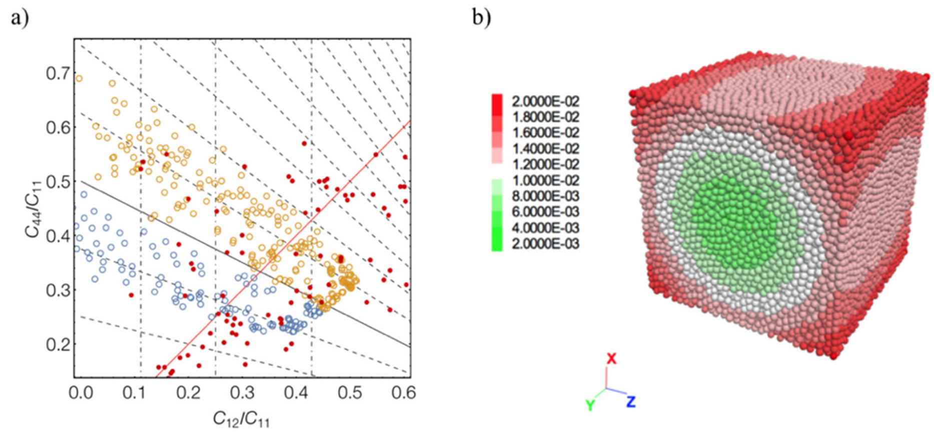

Figure 5. (a) Elastic behavior in the DEM model (open circles) compared with cubic materials (red dots). Below the black line (blue circles) is Z < 1 and above (gold circles) Z > 1, (b) Displacement field in an assembly subjected to strains ε_{yy} and ε_{xz}.

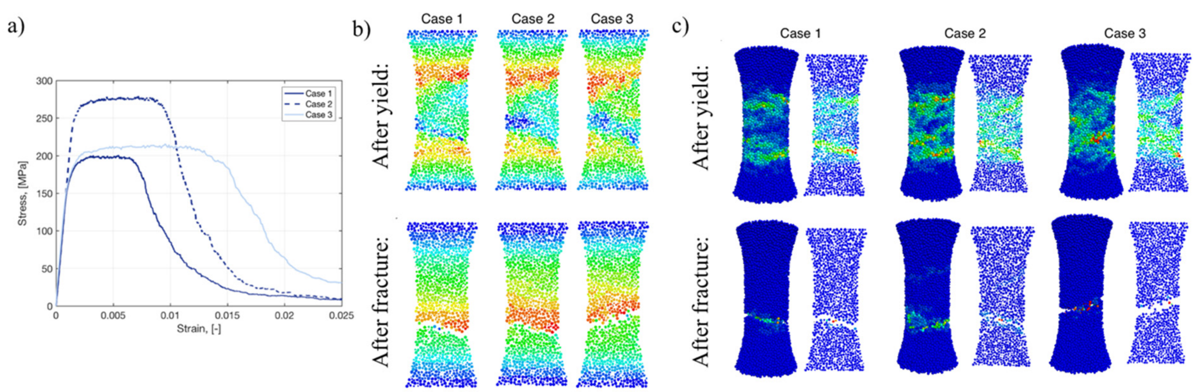

Figure 6. (a) Stress-strain curves for Case 1 (bonds break in tension), Case 2 (bond breakage distributed nearly equally), and Case 3 (bonds break in shear); (b) Results of the d_2^{min} analysis in assembly cross-section; (c) Results of local cage deformation analysis.

formation of shear bands with increased shear deformation of bonds and suggest an interplay between two deformation mechanisms – formation of voids with bonds breaking in tension (Case 1) and shear banding when bonds deform in shear (Case 3).

Isotropic plasticity with hardening

The results of applying different hardening schemes in DEM are shown in Figure 7, and compared to the plastic deformation (up to 10% strain) of Nimonic 75 monotonically loaded in tension at the temperature of 600°C. Although all hardening schemes agree well with the experiments initially, none of the models reached a strain larger than 8%. Overall, the model seems relatively insensitive to how hardening is implemented. Ductility is limited by the threshold for bond breakage and because the bond network is not "rewired" as the deformation

 https://doi.org/10.1557/adv.2017.430

continues (i.e., few new bonds are formed during shear). Work to address these issues and achieve higher ductility is ongoing.

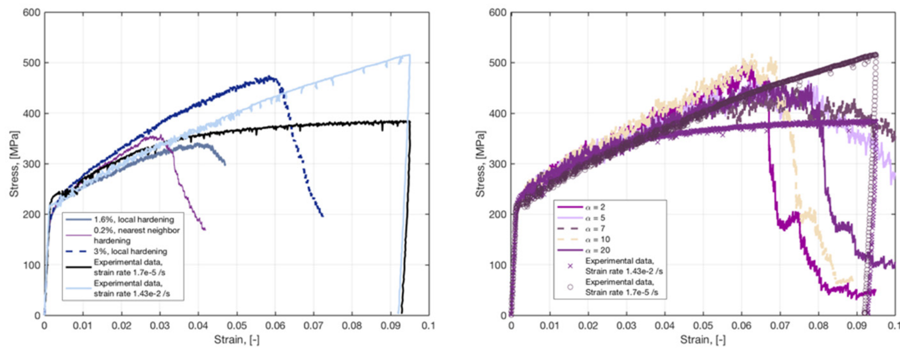

Figure 7. Stress-strain responses in DEM simulations with various hardening schemes: large assembly and local, nearest, and next-nearest neighbor hardening scheme (left); small assembly with exponential decay hardening distribution, smaller values of α correspond to more bonds being hardened (right).

CONCLUSIONS

This paper proposes the discrete element method as a new paradigm for enabling the mesoscale modeling of emergent damage phenomena in continuum materials. One model demonstrated the ability to capture the anisotropic elastic response of a number of cubic materials. An isotropic plasticity model reproduces emergent shear bands characteristic for non-hardening amorphous alloys. The model of isotropic plasticity with hardening agrees well with experimental data for a nickel alloy at small strains, but predicts failure at smaller deformations than those observed in physical experiments. Limitations of all three models suggest a need for more complex and potentially non-pairwise interactions between the DEM elements.

ACKNOWLEDGMENTS

This material is based upon work supported by the Department of Energy National Energy Technology Laboratory under Award Number(s) DE-FE0024065.

REFERENCES

1. A. Pineau and S.D Antolovich, *Eng. Fail. Anal.* **16(8)**, 2668-2697 (2009).
2. P. A. Cundall, O. D. Strack, *Géotechnique* **29(1)**, 47–65 (1979).
3. S. A. Silling, *J. Mech. Phys. Solids* **48**, 175-209 (2000).
4. M. Braun and J. Fernández-Sáez, *Int. J. Fracture* **197(1)**, 81-97 (2016).
5. T. M. Evans and J. D. Frost, *Int. J. Numer. Anal. Met.* **34(15)**,1634–1650 (2010).
6. D. Potyondy and P. Cundall, *Int. J. Rock Mech. Min*. **41(8)**, 1329–1364 (2004).
7. Y.-H. Wang, D. Xu, and K. Y. Tsui, *J. Geotech. Geoenviron.* **134(9)**, 1407-1411 (2008).
8. T. Yuanqiang, D. Yang, and Y. Sheng, *J. Eur. Ceram. Soc.,* **29.6** 1029-1037 (2009).
9. W. Leclerc, H. Haddad, and M. Guessasma, *Int. J. Solids Struct.* **108**, 98-114 (2017).
10. J. J. Kruzic, *Adv. Eng. Mater.* **18**, 1308-1331 (2016)
11. G. Simmons and H. Wang, Single crystal elastic constants and calculated aggregate properties: a handbook, 2nd ed. (M.I.T. Press, Cambridge, 1971)